Asian J Biol Life Sci., 2026; 15(2):530-548.
https://ajbls.com

Research Article

Bio-Fabrication of Silver Nanoparticles: *Murdannia pauciflora* (G. Brückn) Structural Analysis and Multifunctional Biological Properties

Vanajakshi L, Dupadahalli Kotresha*

Department of Studies in Botany, Davangere University, Shivagangothri, Davangere, Karnataka, INDIA.

ABSTRACT

Background: *Murdannia pauciflora* is an ethnomedicinally important plant known for its diverse therapeutic properties. This study reports, for the first time, the green synthesis of Silver Nanoparticles (AgNPs) using aqueous extract of *M. pauciflora* and evaluates their phytochemical composition and biological activities. **Materials and Methods:** Preliminary phytochemical screening revealed the presence of phenols, alkaloids, tannins, glycosides, flavonoids, and saponins. GC-MS analysis identified 98 bioactive compounds, indicating the rich phytochemical profile of the plant extract and its suitability for nanoparticle synthesis. The synthesized AgNPs were characterized using UV-visible spectroscopy, FTIR, XRD, SEM, EDX, DLS, zeta potential analysis, and TEM. Characterization results confirmed the successful formation of stable nanoparticles with a Face-Centered Cubic (FCC) crystalline structure and predominantly rectangular morphology. **Results:** The AgNPs exhibited an average particle size of approximately 12 nm and a zeta potential value of -30 mV, suggesting good stability and uniform surface distribution. Biological studies demonstrated that AgNPs possessed notable pharmacological activities. Cytotoxicity evaluation against pancreatic cancer cells showed an IC_{50} value of 500 µg/mL, whereas no inhibitory effect was observed against HepG2 liver cancer cells. **Conclusion:** The nanoparticles also exhibited significant α-glucosidase inhibitory activity with an IC_{50} value of 78.44 µg/mL, indicating potential antidiabetic properties. Furthermore, antioxidant activity was observed with a free radical scavenging IC_{50} value of 82.65288 µg/mL. Overall, the green-synthesized *M. pauciflora* AgNPs demonstrated promising antioxidant, antidiabetic, and cytotoxic activities, highlighting their potential applications in biomedicine, cancer therapy, drug delivery, and antidiabetic formulations.

Keywords: AgNPs, Biomedical Activities, Characterization, *Murdannia pauciflora*, Phytochemical.

Correspondence:
Dupadahalli Kotresha
Department of Studies in Botany, Davangere University, Shivagangothri, Davangere-577007, Karnataka, INDIA.
Email: dkotresh@davangereuniversity.ac.in

Received: 13-04-2026;
Revised: 28-05-2026;
Accepted: 09-07-2026.

INTRODUCTION

The past few decades have seen a significant increase interest in nanomaterials (1-100 nm materials) across a wide range of industries, including biomedicine, energy storage, catalysis, and sensors (Xu *et al*., 2020). Industry such as food, pharmaceuticals, and agriculture, due to their distinct physicochemical characteristics (Sheme *et al*., 2023). The salts of certain metals, such as Copper (Cu), Iron (Fe), Gold (Au), Silver (Ag), Platinum (Pt), and Palladium (Pd), are used to create metal nanoparticles. AgNPs have several advantages over other metallic nanoparticles. Although many are classified as "AgNPs," some have a high concentration of Ag2O due to the large ratio of surface to bulk Ag atoms. Over the past 10 years, AgNPs have found employment in a variety of medical and technological gadgets, surgical tools, bone cements, surgical masks, and other products. Additionally, wounds are treated with a specific quantity of ionic silver. Consequently, burns and wounds are treated using AgNPs. Molecular labeling uses AgNPs because of their large scattering cross sections and surface plasmon resonance. Thus, a large number of AgNPs are acknowledged for their numerous applications. Because of their remarkable catalytic attributes, it has drawn a lot of attention lately (Mallick *et al*., 2024a; Mallick *et al*., 2021). AgNPs are widely recognized for their potent and extensive antibacterial and cancer-fighting abilities. AgNPs' potential biological functions, such as enhancing wound and bone healing, promoting vaccine immunogenicity, and exhibiting antidiabetic properties, have also been investigated. Better medical applications of AgNPs will be made possible by understanding their biological mechanisms and possible cytotoxicity. Three distinct approaches are possible to create silver nanoparticles: physical, chemical, and biological synthesis. An intriguing substitute for physical and chemical creation of nanoparticles is biogenic synthesis (Gudikandula

DOI: 10.5530/ajbls.20260174

and Charya, 2016). Toxic stabilizing agents and capping agents are used in various physical and chemical processes to maximize reaction conditions, yet they are nevertheless costly and detrimental to humans and the environment. As a result, it is stressed to lower the risk of dangers by creating biosynthetic techniques that use natural items as substrates. Various biological precursors, including secondary metabolites and enzymes, are involved and facilitate the bioreduction reaction in a rapid and environmentally benign manner. Plant extracts from various plant parts, such as bark, peel, callus, leaves, flowers, fruit, stems, seeds, and rhizomes, can also yield nanoparticles of all sizes. According to (Kuppusamy *et al*., 2015), these include spherical, triangular, pentagonal, hexagonal, nanorod, nanoprism, and irregular shapes. *Murdannia pauciflora* G. Bruckn is a member of the Commelinaceae family, which has 650 species spread over 41 genera (Lee *et al*., 2022). There are 55 species in the genus *Murdannia* worldwide. Though Asia has the greatest diversity, it is found widely throughout the warm temperate and tropical regions of the world (Nandikar and Gurav, 2015). Species of the genus *Murdannia* can be observed in grassy slopes and woods throughout Asia, including China and Thailand. The plant is traditionally used to treat skin conditions; the entire plant is indigenous to India and is known as a few-flowered dew flower (Malavika and Thenmozhi, 2023). Alkaloids, phenols, flavonoids, tannins, and saponins are chemicals found in *Commelina nudiflora* that may be a source of nutrition for both people and animals (Ujowundu *et al*., 2007). In this study, we used whole plant extract of *M. pauciflora* (*M. pauciflora* AgNPs) to study the formation of AgNPs. UV-visible spectroscopy, Fourier-Transform Infrared (FTIR), X-ray Diffraction (XRD), Dynamic Light Scattering (DLS), zeta potential, Scanning Electron Microscopy (SEM) in conjunction with Energy Dispersive X-ray (EDX), Transmission Electron Microscopy (TEM), and other techniques were used to ascertain the size, shape, morphology, and stability of *M. pauciflora* AgNPs. The antioxidant activity of the *M. pauciflora* AgNPs was evaluated using the DPPH and ferric chloride method. The disc diffusion method for antimicrobial activity, α-glucosidase inhibitory activity, and MTT assay (Panc-1 and HepG2) were used to assess the antimicrobial, antioxidant, antidiabetic and anticancer properties of the *M. pauciflora*. AgNPs.

MATERIALS AND METHODS

Collection of *M. pauciflora* (G. Brückn.) Plant Material

Murdannia pauciflora (G. Brückner) whole plant (Figure 1) was collected from Sirsi, Uttara Kannada district of Karnataka, India. During January, the herbarium was identified by A. N. Sringeswara, curator at the Mahatma Gandhi Botanical Garden, University of Agricultural Sciences, GKVK, Bangalore, collected the specimen under no. C001, with Accession number UASB 5,774.

Plant Extract Preparation

The plant surface was thoroughly washed with running tap water to eliminate any particulate matter and contaminants. The plants are shade-dried, and the dried samples were grounded by a mechanical grinder. About 25 g of plant powder were extracted using the Soxhlet method using several solvents at varying temperatures. Several iterations of the extraction procedure were conducted to obtain enough extract for more research. The semisolid extract was kept at 4°C until it was needed again after the crude extract was allowed to evaporate and then exposed to preliminary phytochemical analysis to determine its primary and secondary metabolites (Figure 2).

Qualitative Phytochemical Analysis

The following conventional methods were carried out to test the extract for the presence of bioactive chemicals from the studies of (Banu and Cathrine, 2015; P M *et al*., 2025; Praveen and Kakkalameli, 2025a).

GC-MS Analysis of *M. pauciflora*

GC-MS Analysis of whole plant extract of *M. pauciflora* was performed using QP2010S, Shimadzu, Japan, Mass Spectrometer (GC) and Gas Chromatograph (MS) enhanced with an electron ionization detector. An EC-5 column (0.25 µL, 30 m, 0.25 mm) and a 2-mm direct injector were included with the chromatograph. A 2-mm direct injector liner was used to inject a total of 2 µL of sample. The temperature was set to begin at 60°C for 2 min and then increase to 450°C at a rate of 20°C/min (Chakraborty *et al*., 2022). All specimens were injected straight into the capillary column using a 2-mm injector. The identification of the chromatographic peaks was achieved by their relative retention times, and the mass spectrometric analysis was conducted by precisely identifying the compounds through comparison of the spectral data with the National Institute of Standards and Technology library (RC & Kakkalameli, 2025; Vanajakshi *et al*., 2025).

Pilot Study

Concentration optimization

We evaluated the sample for three different concentrations of plant extract and 1 Mm $AgNO_3$ in the ratio of 1:9, 2:8, and 3:7 distinct concentrations for 10 mL of sample (plant extract + $AgNO_3$) with the aim to find the optimal amount of extract required for the effective generation of AgNPs. And the 2:8 ratio concentration produced the best outcomes.

Optimization of pH

The ideal pH is necessary for the best synthesis of AgNPs. The samples (2:8) were treated with three different pH values: 3.3 (Acidic), 7 (Neutral), 10.1 (Basic) and. The best results were obtained in basic pH.

Temperature optimization

The production of nanoparticles is strongly influenced by temperature. Therefore, 0.1 M $AgNO_3$ solution with a 2:8 ratio treated with three different temperatures -4, 40, and 60°C was used to identify the ideal temperature required for optimizing *M. pauciflora* AgNPs yield within the ideal time frame. At 60°C, the best synthesis was discovered.

Bio-fabrication of Ag NPs from the aqueous extract of *M. pauciflora*

The entire plant extract of *M. pauciflora* was used to create silver-nitrate nanoparticles ($AgNO_3$ NPs). 25 g of plant extract and 5 Mm of $AgNO_3$ were produced as a stock solution. Additionally, 1 Mm of $AgNO_3$ was utilized for synthesis, and the solution was made up to the ratio of 2:8, 2 mL of plant extract and 8 mL of $AgNO_3$ solution. It is noted that the color of the reaction combination (leaf extract and silver-nitrate solution) changes with time. The creation of AgNPs is shown by the color changing from pale yellow to brown after 30 min of incubation. The yellow-colored solution gradually turned dark brown after 120 min, due to both the AgNPs' increasing concentration and particle size development (Bhavi *et al*., 2024).

UV-visible spectrum analysis was used to track the Ag^+ ion reduction over time. The reaction mixture was centrifuged to extract the AgNPs. Before characterization, the nanoparticles were resuspended in 95% ethanol after being cleaned three times with deionized water. The green production of nanoparticles has been kept at a pH of 10.1 at temperature of 60°C. Following that, tiny precipitants were separated by centrifugation at 5,000 r.p.m. for 30 min. After the supernatants were removed, the precipitates were agitated with distilled water and ground with a mortar and pestle to achieve a homogeneous texture for further analysis and characterization.

Characterization of *M. pauciflora* AgNPs

UV-visible spectroscopy analysis

Using a dual-beam UV-9600 a spectrophotometer (Shanghai, China), the generated nanoparticles of *M. pauciflora* were exposed to UV-visible light. Followed by introduced to a cuvette, AgNPs nanostructures made from the entire plant extract were examined for optical absorbance over a 200-800 nm wavelength range. To provide a thorough assessment of the nanoparticles, the acquired spectrum data were then graphically depicted, with absorbance intensity mapped in the *Y*-axis and wavelength values plotted in the *X*-axis (Karadakatti *et al*., 2024).

FTIR

FTIR spectrum, which is made up of absorption peaks that match the frequency of vibrations between the atoms' bonds, stands in for the signature of the nanoparticles. Because every kind of nanoparticle has a different atom configuration, we may use the FTIR spectra to determine if functional groups are present within the nanoparticles. It is possible to determine the functional groups in the nanoparticles by looking at the size of the peaks in the spectrum. AgNPs made from *M. pauciflora* the evaluation was conducted using a Thermo Fisher Scientific FTIR spectrophotometer (Waltham, MA, United States). To create a compacted pellet, Potassium Bromide (KBr) was mixed with the dried powder of manufactured nanoparticles. Identification of infrared absorption bands was made possible by the evaluation of the KBr pellets within the 400-4,000 cm^1 spectral range. Using spectral data analysis in the 400-4,000 cm^1 region, the existence of functional biomolecules in the sample was confirmed, allowing a thorough description of the chemical makeup of the nanoparticles (Jaast and Grewal, 2021; Praveen and Kakkalameli, 2025b).

XRD analysis

To create the powder XRD pattern, the dried powder of synthesized *M. paucifora* AgNPs is exposed to an X-ray diffractometer (Rigaku Miniflex 600, SmartLab SE, Tokyo, Japan) at 40 kV and 30 mA, with a scanning rate of 40° min-1, at angles of 2θ that range from 20 to 80° (Thokchom *et al*., 2023).

SEM and EDX analysis

Topological structure and elemental composition of *M. pauciflora* AgNPs were detected by SEM paired with an EDX device (JEOL, JSM IT 500 LA, Peabody, MA, United States). Simply, *M. pauciflora* AgNPs were stuck to the stub using carbon tape, fixed, and flashed with gold. After that, the prepared stub was put in the instrument chamber for the analysis (Nayaka *et al*., 2020).

Zeta potential and DLS analysis

To evaluate the electrostatic charge and size distribution of *M. pauciflora* AgNPs. The samples are subjected to the zeta potential and DLS analysis using HORIBA SZ100, Kyoto, Japan. The uniform distribution of the *M. pauciflora* AgNPs is achieved by using ultrasonic agitation; the mixture was centrifuged for 20 min at 6,000 r.p.m. at 3.4 eV, which is essential for understanding behavior and possible applications (Bhavi *et al*., 2024).

TEM analysis

Using an FEI Tecnai G2 F30 system (Beijing, China), TEM was used to examine the detailed imagery of the *M. pauciflora* AgNPs, displaying their internal structure and morphology at an enhanced resolution. A 5 µL aliquot of the ZnO nanoparticle suspension was placed onto a copper grid and dried for 48 hr. Following the examination of the nanoparticles at an accelerating voltage of 300 keV, high-resolution pictures were obtained at a magnification range of 7,000×8,000, enabling accurate characterization of their morphological and structural characteristics (Abbigeri *et al*., 2024).

Biological activities

Cytotoxicity

Cell culture

The National Centre for Cell Sciences in Pune, India provided the human pancreatic (PANC1) and liver cancer cell lines (HepG2). These cells were kept in Dulbecco's Modified Eagle Medium supplemented with 10 mm 4-(2-hydroxyethyl)-1-p iperazineethanesulfonic acid, 0.1 mm nonessential amino acids, 1 mm sodium pyruvate, 1.5 g/L glucose, 2 mm l-glutamine, and a balanced salt solution containing 1.5 g/L Sodium Carbonate (Na_2CO_3). To encourage cell proliferation, 10% fetal bovine serum (Gibco, United States) was also added. To avoid microbiological contamination, penicillin and streptomycin were added at a dosage of 100 international units/100 µg/mL. The cells were kept in a humidified incubator with 5% Carbon Dioxide (CO_2) at 37°C to provide ideal physiological conditions for growth and survival.

Evaluation of cytotoxicity by MTT Assay

The inhibition percentage was calculated by MTT assay to assess the viability of cells. A 96-well microplate was seeded with cultured cells (1×10^5) and incubated for 48 hr at 37°C in a humidified 5% CO_2 incubator. After incubation, 100 µL of different concentrations (0-160 µg/mL) of AgNPs produced from *M. pauciflora* were added to each well after the monolayer was rinsed with fresh media. For additional exposure, the cells were kept under the same settings. After discarding the culture media, 100 µL of MTT reagent was added to each well, and the mixture was then incubated for an additional 4 hr at 37°C. To ensure precise measurement, 100 µL of Dimethyl Sulfoxide (DMSO) was added to dissolve the formazan crystals after the supernatant was removed. The cell viability percentage was computed using the optical absorbance measured at 590 nm. A dose-response curve was used to analyze the data and calculate the IC_{50} value,

Figure 1: Showing (A) Habitat, (B) Front view of the flower, (C) Side view of the flower.

Figure 2: Green synthesis of silver nanoparticles.

which represents the concentration needed to inhibit 50% of cell proliferation (Mandour *et al*., 2023).

Antidiabetic activity

α-glucosidase inhibition

The α-glucosidase activity of *M. pauciflora* was determined by following the previously reported assays. Phosphate buffer (50 mm, pH 6.9) was combined with 50 µL of α-glucosidase (1 U/mL) from yeast (SRL, Bangalore, India) and subjected to different levels of concentration. AgNPs (0-125 µg/mL) of *M. pauciflora* for 10 min at 37°C. 50 µL of 5 mm pnitrophenyl-D-glucopyranoside was added to the phosphate buffer to initiate the reaction. After 30 min at 37°C, the enzymatic process was stopped by adding 1 M Na_2CO_3. At 405 nm, absorbance was measured. Acarbose was used as a positive control, and the percentage of inhibition was computed and reported as IC_{50} values (Sukanya *et al*., 2017).

Antioxidant activity

DPPH assay

Different volumes of concentration of *M. pauciflora* AgNPs (0-250 µg/mL) are mixed with 2 mL of DPPH (100 µm), and the final volume is adjusted to 3 mL with methanol, and the reaction mixture is allowed to incubate in a dark chamber for 45 min. At the end of incubation period, absorbance was recorded using a spectrophotometer (Shimadzu UV-1800, Kyoto, Japan) at 517 nm against the blank (Without sample/Standard). Free radical scavenging capacity of the samples were calculated and expressed in IC_{50} values in comparison with BHT as a standard antioxidant (Baliyan *et al*., 2022).

RESULTS AND DISCUSSION

Qualitative Phytochemical Analysis

The phytochemical study reveals that the presence of phenols, flavonoids, alkaloids, tannins, saponins, and glycosides in *M. pauciflora's* methanolic extract, whereas steroids are absent. The lack of steroids and alkaloids in the aqueous extract indicates that they are extracted using organic solvents, but the chloroform extract solely reveals the existence of saponins. These results highlight the importance of solvent choice in phytochemical research, which in turn affects *M. pauciflora's* potential therapeutic uses. Additional studies may yield a more profound understanding of its pharmacological advantages (Table 1) (Huq, 2015).

GC-MS Analysis

The GC-MS analysis of the aqueous extract shows approximately 98 bioactive compounds based on their retention time and area percentage, as shown in (Table 2). The compound bisabolol oxide b <alpha-> has a high area percentage of 20.16 and RT of 32.500, lactic acid RT 4.035, Pimelic ketone RT 5.859, cyclohexane <1,2-dioxo-> RT 7.144, Benzenecarboxylic acid RT 9.903, syringaldazine RT 11.583, Cineole <1.4-> RT 12.045, December 9-enoic acid RT 13.795, isoborneol <8-isobutyryloxy-> RT 16.151, Incensole RT 18.455, hexadecanoic acid <n-> RT 20.115, pyrazine <2-methoxy-> RT 25.725, valeranone, RT 26.900, dihydrotagetone RT 27.827, decamethylcyclopentasiloxane RT 28.039, Eicosene RT 30.190, Tricos-(9Z)-ene RT 33.667, Phytol RT 36.735, tetracontane <n-> RT 40.114. The GC-MS studies

on *Murdannia simplex* and *Murdannia lanuginosa* the root methanolic extract reveal that three compounds in six compounds in *M. simplex* and three compounds in *M. lanuginosa* and these plants have properties like an antimicrobial, antiproliferative and anti-inflammatory activities and also used as a fungicide due to the presence of compounds like H-Pyran-4-one, 2, 3-dihydro-3,5-dihydroxy-6-methyl, salicylaldehyde and Azine (Nandikar *et al*., 2018). The investigations by the researchers found that the methanolic and hexane extract of *M. bracteatea, M. lanuginose, M. simplex* the GCMS results shows bioactive compounds like stigmasterol, α-tocopherol, β- β-sitosterol in *Murdannia bracteata*, diphenyl-, 2-oxide 3,4-diphenylfurazan 2-oxide diphenylfuroxan and diphenylfurazan N-oxide furazan in *M. simplex* and *M. lanuginosa* shows the compounds like azine and salicylaldehyde (Figure 3) (Patrick and Bakhari, 2020).

Characterization of *M. pauciflora* AgNPs

Bio-fabrication of Ag NPs from the aqueous extract of M. pauciflora

Murdannia pauciflora AgNPs were synthesized by incubation the reaction mixture at 60°C for 30 min, allowing plant phytochemicals to reduce Ag^+ ions (Figure 4a). The pH was adjusted to 10.1 with 1 N NaOH to enhance reduction efficiency and nanoparticle formation. After 10 min of stirring, the color changed from pale yellow to dark brown, confirming *M. pauciflora* AgNP formation. The proposed mechanism (Figure 4b) illustrates how the alkaline medium and phytochemicals drive Ag^+ reduction and nanoparticle growth. The nanoparticles were purified by centrifugation at 5,000 r.p.m. for 30 min.

UV-visible spectroscopy analysis

The color shifts from pale yellow to brown, indicating the creation of nanoparticles. Additionally, the UV-visible spectrum provided spectroscopic confirmation. The intensity of *M. pauciflora* AgNPs ranged from approximately 350 to 485 nm, with a confirming spot at 405 nm (Figure 5). The findings of (Mukherji and Mondal, 2017), this peak results from the interaction between the Surface Plasmon Resonance (SPR) of metallic Ag+ and SPR, which is caused by the collective oscillation of conduction electrons on the NP surface when activated by light at a particular wavelength. The peak that emerged is consistent with earlier studies that discovered AgNPs' absorption at 406 nm (Bhavi *et al*., 2025). *Murdannia pauciflora* AgNPs' size has been connected to their intensity in the UV-visible spectrum. The presence of secondary metabolites in plants serves as a reducing agent and converts Ag^+ to Ag^+. Similar SPR peaks are observed in other studies (Mohamad *et al*., 2021).

FTIR

FTIR spectrum of *M. puacifora* AgNPs exhibited the characteristic peaks ranging from 4,000 cm^{-1} to 600-1. The peaks 3,234.29, 3,138.63 cm^{-1} attributed to O-H Stretching, the peaks 3,101.68, 3,005.20, 2,957.99, 2,713.71 attributed to C-H Stretching, 1,575.19 attributes to C=C Stretching, and the Peaks 2,251.84, 1,393.37, 1,011.64, 780.18, 665.65 are attributed to N = C = O Stretching, O.-H. Bending, S = O Stretching, C=C Bending and C-Cl Stretching corresponding to alcohol, carboxylic acid, aromatic hydrocarbon. Alkene, alkene, alkyl halide, sulfoxide, aldehyde, isocyanate and cyclic alkane. These functional groups serve as a surface coating and promote in the efficient stabilization of nanoparticles and the plant's phytochemicals operate as a capping agent during synthesis (Akintelu *et al*., 2020). These results are consistent with the discovery that AgNPs of *Commelina erecta* stretch vibrations of -OH groups in the peaks between 3,500 and 300 cm^{-1}. These O-H groups are attributed to C-H stretching of aliphatic structures at 2,895 and 2,840 cm^{-1}, xylan, cellulose, and hemicellulose, corresponding to vibrations of -CH and -CO at 1,400-900 cm^{-1} (Table 3). *Commelima forskaolii* has disulfide amino and hydroxyl groups at peaks of 3,289.50, 1,617.18, 1377, 1,030.27, and 464.86 (Figure 6) (Vijay *et al*., 2023).

Table 1: Preliminary Qualitative Phytochemical Analysis of *M. pauciflora* extracts.

Sl. No.	Phytochemical tests	MPM	MPA	MPC
1.	phenols	+	+	–
2.	alkaloids	+	–	–
3.	flavonoids	+	+	–
4.	tannins	+	+	–
5.	saponins	+	+	+
6.	glycosides	+	+	–
7.	steroids	–	–	–

Abbreviations: +=Present and—= Absent; A=Aqueous; C=Chloroform, MP = *M. pauciflora*; M=Methanol.

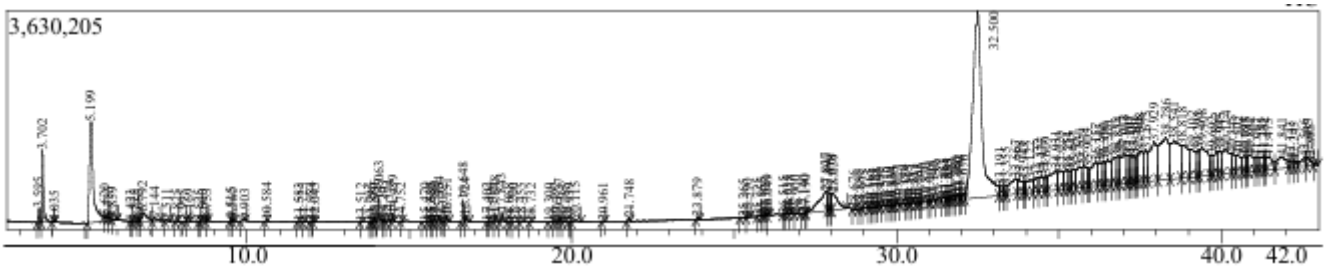

Figure 3: Showing chromatogram of *M. pauciflora* aqueous extract.

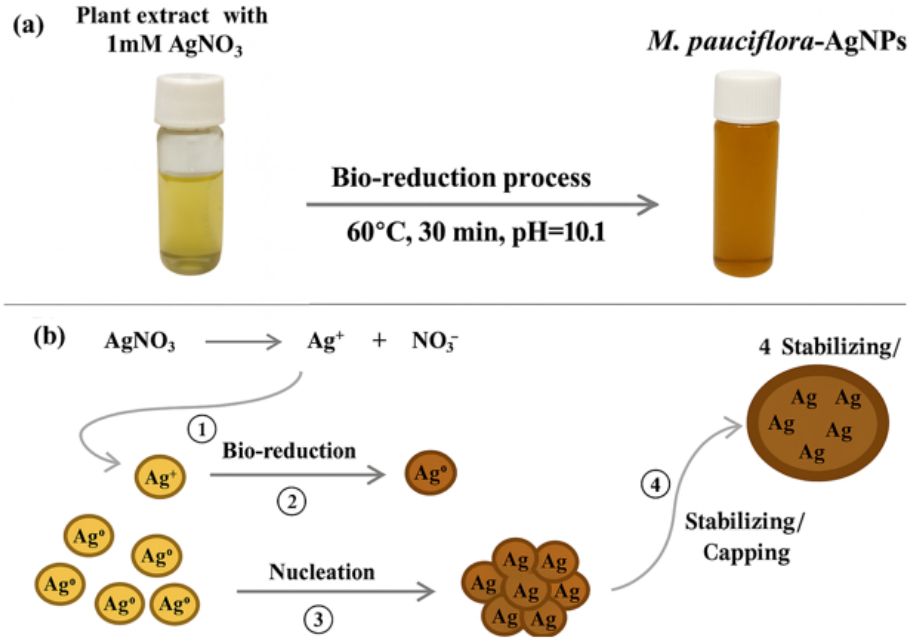

Figure 4: (A) Showing color shifting from pale yellow to brown color. (B) Mechanism of how plant phytochemical helps in synthesis of *M. pauciflora* AgNPs.

XRD analysis

The XRD diffractogram displayed prominent peaks at 2θ = 28.28°, 32.15°, 38.16°, 40.44°, 44.16°, 46.16°, 50.15°, 64.60°, 77.46°, and 81.61°, which correspond to the crystallographic planes (004), (101), (111), (112), (103), (104), (200), (220), (311) and (222), respectively (Figure 7). Among these, the characteristic reflections of metallic silver were clearly observed at 38.16° (111), 44.16° (200), 64.60° (220), 77.46° (311), and 81.61° (222). These values are in excellent matches with the standard diffraction data for face-centered cubic (FCC) silver reported in JCPDS File no. 00-004-0783 (Bhavi *et al*., 2024). Using the Scherrer equation, the average crystallite size of the synthesized nanoparticles was estimated to be approximately 12.0 nm. Additionally, the diffraction peaks obtained at 38.17°, 44.36°, 64.51°, 77.43°, 81.56°, and 98.06° perfectly match the standard metallic Ag reflections of FCC Ag, further confirming the successful formation of phase-pure Silver Nanoparticles (AgNPs). The absence of additional peaks indicates that no secondary or impurity phases were present, supporting the high crystallinity and purity of the synthesized AgNPs.

The detailed XRD analysis in the present study offers meaningful insights into the crystallographic features and the potential applications of the synthesized nanoparticles. Similarly, our results are consistent with those documented for *Camellia sinensis* mediated silver nanoparticles by (Ali *et al*., 2022; Mehta *et al*., 2017).

SEM analysis

The SEM investigation of *M. pauciflora* AgNPs reveals information on morphology and surface distribution. The synthesized AgNPs range in size from rod to rectangular, with aggregates containing clusters of nanoparticles. Examining the agglomerated masses revealed several nanoparticle aggregates. Nanoparticles could exist independently or in clusters. Some had a rod shape with an average size of 12.0 nm, as seen in (Figure 8). Some aggregation was observed, which is common in green synthesis methods because the bioactive molecules in the plant extract may not offer the same steric protection as synthetic capping agents (Johnson and Prabu, 2015; Oseghale *et al*., 2025). found that *Commelina benghalensis* SEM investigation revealed the formation of reasonably spherical and homogenous Ag nanoparticles with diameters ranging from 13 to 51 nm.

EDX analysis

EDX micro examination involves evaluating the energy and intensity distribution of X-ray signals generated by an electron beam on a specimen (Figure 9). Depicts the peaks inferred during EDX analysis. The spectra show that the synthesized AgNPs contain Ag, as well as additional elements like Manganese (Mn), Sodium (Na), Calcium, Potassium (K), Sulfur (S), and Silicon (Si). The other elements act as capping organic agents on the surface of the silver nanoparticles (Bhav *et al*., 2024). The present study's EDX examination confirmed the presence of silver nanoparticles

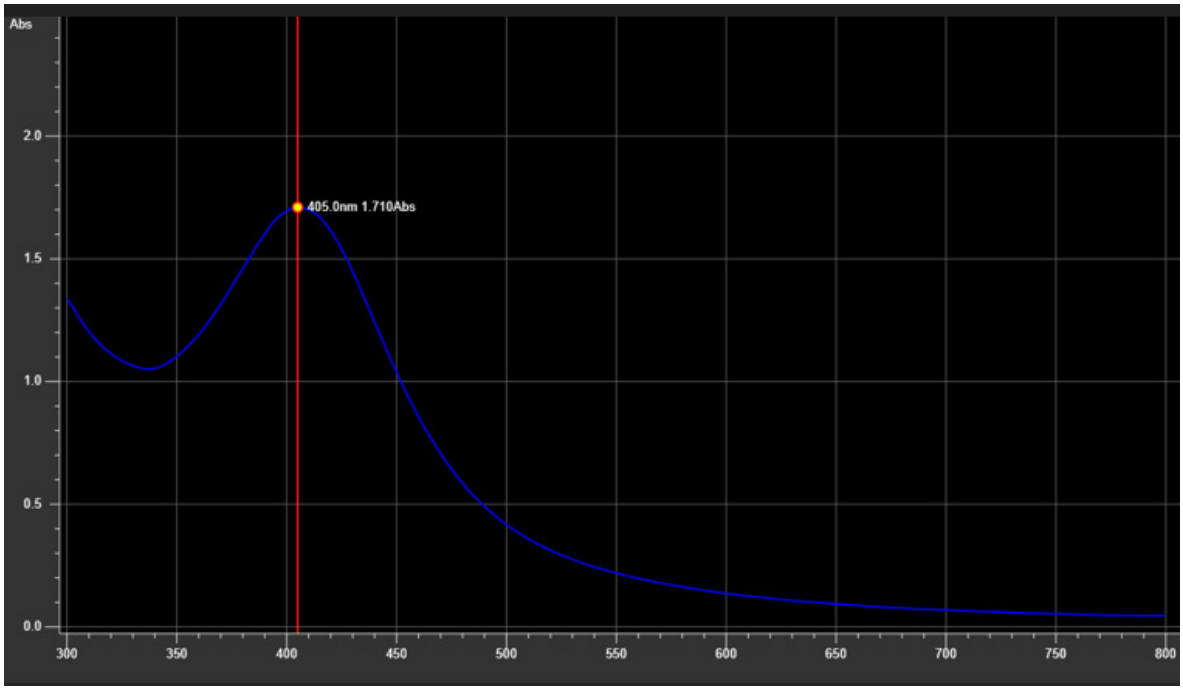

Figure 5: UV-vis Analysis of *M. pauciflora* AgNPs.

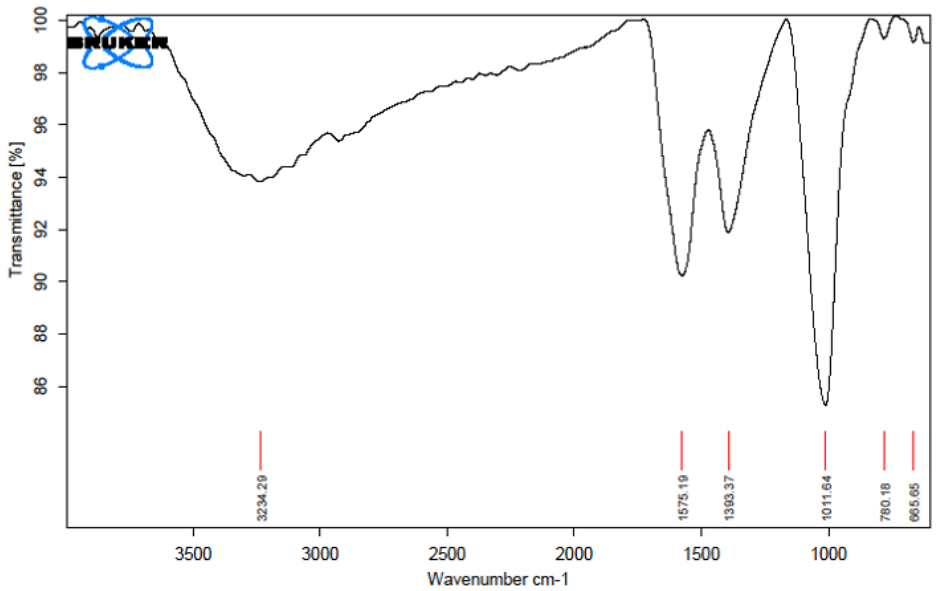

Figure 6: Fourier-Transform Infrared (FTIR) spectrum of *M. pauciflora* AgNPs.

from *M. pauciflora* and revealed high signal energy peaks for silver atoms.

Zeta potential and DLS analysis

The physicochemical characterization of the synthesized nanoparticles was evaluated through zeta potential and particle size distribution analyses, which are critical indicators of colloidal stability and uniformity. The zeta potential graph (Figure 10A) shows a sharp, symmetrical Gaussian-shaped peak centered near the negative potential region, indicating a highly charged particle surface. The relatively narrow and smooth peak suggests that the nanoparticles possess a consistent surface charge, which supports the formation of a stable colloidal system. Zeta potential plays a crucial role in assessing the colloidal stability of nanoparticles and understanding their suitability for various applications (Vanlalveni *et al.*, 2021). A higher magnitude of zeta potential-typically more negative than −30 mV or more positive than + 30 mV is associated with strong electrostatic repulsion among particles, thereby minimizing aggregation. The peak pattern observed here confirms that the synthesized nanoparticles exhibit good dispersion stability, which is essential for their biological and catalytic applications. In the present study, the synthesized nanoparticles exhibited a distinctly negative zeta potential, which can be attributed to the presence of negatively

charged capping agents on their surface. These biomolecules provide electrostatic repulsion between particles, preventing agglomeration and thereby maintaining long-term colloidal stability (Khandel *et al*., 2018). The particle size distribution profile (Figure 10B) further complements these findings by revealing a uniform and narrow size range, as evidenced by the compact histogram and the steep cumulative distribution curve. Most particles fall within a controlled nanoscale region, demonstrating that the synthesis process successfully limited polydispersity. A narrow distribution is a hallmark of effective nucleation and growth mechanisms during nanoparticle formation. Such uniformity ensures reproducibility in functional properties, including surface reactivity, drug-loading behavior, and antimicrobial efficiency. Together, the zeta potential and DLS results confirm that the nanoparticles synthesized in this study are stable, uniformly dispersed, and structurally consistent. These

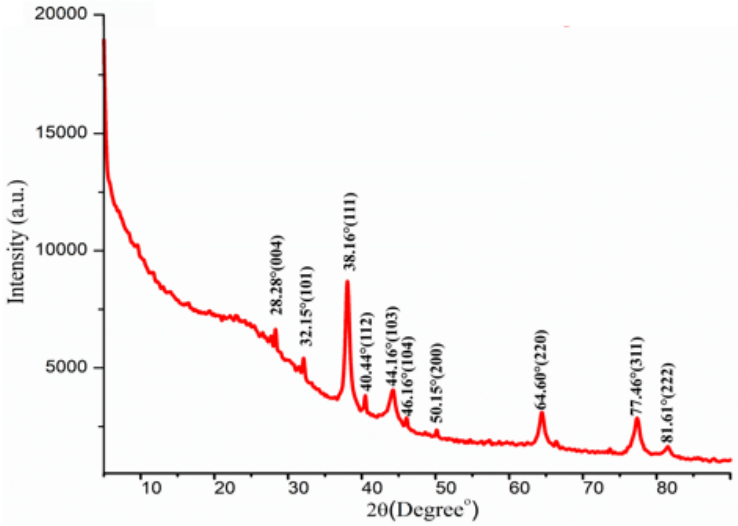

Figure 7: X-ray Diffraction (XRD) Analysis of *M. pauciflora* AgNPs.

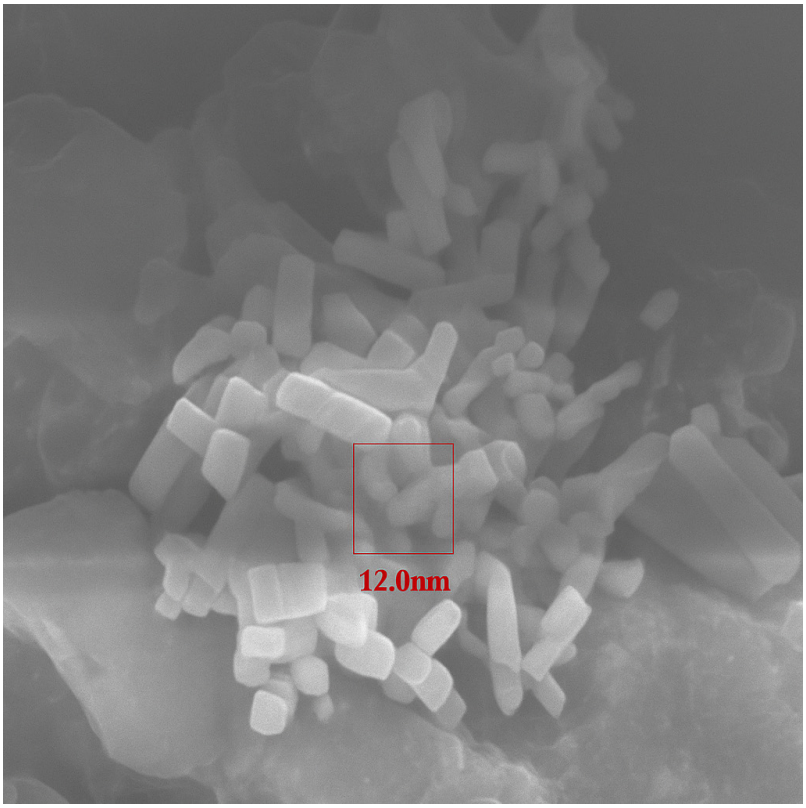

Figure 8: Scanning Electron Microscopy (SEM) image of *M. pauciflora* AgNPs.

Table 2: GC-MS Analysis of Bioactive compounds from *M. pauciflora*.

Peak#	R. Time	Area	Area%	Similarity	Base m/z	Compound name
1	3.595	828,568	0.28	96	45.00	Butadienol <2.3->
2	4.035	2106	0.00	42	43.95	geranyl isovalerate
3	4.035	14,762,377	4.95	98	43.95	lactic acid
4	5.620	85,565	0.03	95	42.00	butyrolactone <gamma->
5	5.735	15,240	0.01	76	108.05	pyrazine <2,6-dimethyl->
6	5.859	53,930	0.02	81	98.00	pimelic ketone
7	6.423	9,885	0.00	62	43.00	isobutyrate <heptyl->
8	6.525	37,122	0.01	64	45.00	ethanoic acid
9	6.665	60,428	0.02	66	117.00	malate <diethyl->
10	6.792	1,592,782	0.53	84	43.00	Butan-2-one <3-mercapto->
11	7.144	377,836	0.13	85	70.00	cyclohexane <1,2-dioxo->
12	7.511	66,331	0.02	75	68.00	Cyclohexen-1-one, <2->
13	7.825	23,163	0.01	79	71.05	tetrahydrofurfuryl alcohol
14	7.995	21,410	0.01	53	115.05	hexanal <dimethyl-> acetal
15	8.169	42,994	0.01	70	43.00	furanone <4-acetoxy-, 2,5-dimethyl-, 3(2H)->
16	8.525	11,881	0.00	57	43.95	butyroin
17	8.600	54,170	0.02	56	85.00	ipsdienol
18	8.753	30,459	0.01	83	57.05	undecane <n->
19	9.515	114,434	0.04	74	43.00	acetate <2,4-dimethyl-, ethyl-, 1,3-dioxolane>
20	9.903	76,453	0.03	61	105.05	Benzenecarboxylic acid
21	10.584	26,207	0.01	69	86.00	triethylamine
22	11.583	22,451	0.01	30	281.00	syringaldazine
23	11.725	23,819	0.01	43	73.05	Acsantol isomer I
24	11.984	74,675	0.03	89	150.05	guaiacol <4-vinyl->
25	12.045	28,248	0.01	65	43.00	cineole <1.4->
26	13.512	19,202	0.01	84	41.00	caryophyllene <(E)->
27	13.795	10,318	0.00	49	45.05	December 9-enoic acid
28	13.850	28,716	0.01	44	69.05	cinnamaldehyde <alpha-hexyl->
29	13.936	170,365	0.06	36	73.00	pentanol, <3-Methyl-3->
30	14.063	1,031,212	0.35	97	55.00	tridecanol <n->
31	14.203	145,803	0.05	88	132.05	curcumene <alpha->
32	14.374	143,996	0.05	91	119.10	Funebrene <alpha->
33	14.489	293,214	0.10	71	191.10	phenylacetate <methyl-, para-tert-butyl->
34	14.752	20,026	0.01	84	69.05	Sesquisabinene
35	15.470	73,232	0.02	53	148.95	phthalic acid, bis(2-ethylhexyl) ester (6CI,8CI)
36	15.635	66,877	0.02	69	151.05	dihydrojasmone
37	15.680	36,423	0.01	62	57.00	valerate <ethyl->
38	15.780	95,535	0.03	72	68.95	callicarpenal
39	16.032	26,081	0.01	64	71.05	linalyl anthranilate
40	16.151	234,578	0.08	79	108.05	isoborneol <8-isobutyryloxy->
41	16.648	906,597	0.30	86	55.00	Tetradec-1-ene
42	16.724	284,948	0.10	93	57.00	propanoate <decyl->

43	17.402	15,383	0.01	59	43.95	decanal <n->
44	17.490	27,956	0.01	51	39.95	vinylcyclohexane <1-acetoxy-, 2 s-butyl->
45	17.843	524,709	0.18	74	124.05	pyrazine <2-isobutyl-, 3-methoxy->
46	18.068	11,400	0.00	59	45.00	Tridec-(2E)-en-1-ol
47	18.200	58,467	0.02	58	70.05	isophorone <2-hydroxy->
48	18.455	51,173	0.02	68	43.00	incensole
49	18.732	16,466	0.01	59	149.05	Rosifoliol
50	19.300	30,306	0.01	49	39.95	cyclohexanemethanol <2,4-dimethyl-> acetate
52	19.939	28,198	0.01	58	70.05	tiglate <isoamyl->
53	20.115	185,576	0.06	90	73.00	hexadecanoic acid <n->
54	20.961	33,092	0.01	70	57.05	butyrate <decyl->
56	25.725	7,593	0.00	36	39.95	pyrazine <2-methoxy->
57	25.855	2159	0.00	50	39.95	menthol
58	26.049	107,712	0.04	34	339.15	Purolan
59	26.515	6,086	0.00	52	57.05	octadecyl chloride
60	26.635	38,449	0.01	50	81.05	Tetrahydroionol isomer II
61	26.900	14,566	0.00	49	125.15	valeranone
62	27.140	40,118	0.01	50	99.10	pulegol <trans->
64	27.827	5,842,843	1.96	41	57.05	dihydrotagetone
65	27.890	1,327,616	0.45	40	57.05	Ambercore isomer I
66	28.039	3,397,594	1.14	39	73.00	decamethylcyclopentasiloxane
67	28.676	24,541	0.01	49	81.05	ethyl menthone <2->
68	28.975	91,572	0.03	53	43.95	n-Tetradecanonitrile
69	29.165	61,444	0.02	58	57.05	citronellyl propionate
70	29.285	66,919	0.02	50	81.05	Palustrol
71	29.378	84,215	0.03	49	95.10	menthyl isovalerianate
72	29.490	60,826	0.02	38	96.05	2-tert-butyl-4-methyl cyclohexanol isomer I
73	29.575	129,964	0.04	57	83.05	octadecanol <n->
74	29.710	90,730	0.03	54	97.05	Pseudodiosphenol
75	29.895	33,996	0.01	46	96.05	Eremophilone <8-hydroxy-dihydro->
76	30.190	143,528	0.05	62	97.05	eicosene
77	30.315	74,374	0.02	57	57.05	tridecanal <n->
78	30.511	166,877	0.06	67	57.05	Octadec-1-ene
79	30.706	55,014	0.02	48	67.00	Oct-2-ene <8-ethoxy-, 2,6-dimethyl->
80	30.870	394,533	0.13	56	69.05	phytol acetate
82	31.555	206,879	0.07	49	69.05	Applelide
83	31.605	198,737	0.07	55	69.00	Timberol, cis-
84	31.655	352,067	0.12	54	95.10	Tetrahydroionol isomer II
85	31.902	555,900	0.19	45	354.95	heptadecanol <n->
86	31.970	248,541	0.08	50	57.05	octadecyl chloride
87	32.070	520,972	0.17	47	39.95	sclareol
88	32.500	60,141,722	20.16	56	178.00	bisabolol oxide b <alpha->
89	33.191	1,181,379	0.40	61	69.00	Hex-2-enal <2-isopropyl-, 5-methyl->
90	33.355	908,647	0.30	55	111.05	ethyl menthone <2->

91	33.667	4,192,656	1.41	67	57.05	tricos-(9Z)-ene
92	33.943	931,845	0.31	64	57.05	Hexadec-(8Z)-enal <14-methyl->
93	35.325	1,418,120	0.48	35	112.10	Labd-(13E)-8,15-diol
94	36.500	4,044,496	1.36	65	111.10	Tetrahydroionol isomer I
95	36.735	4,425,729	1.48	66	71.05	phytol
96	40.114	6,394,222	2.14	69	57.05	tetracontane <n->
97	42.566	1,813,978	0.61	45	85.05	Ambercore isomer III
98	42.885	218,262	0.07	54	83.05	Tetradec-2-enal <trans->

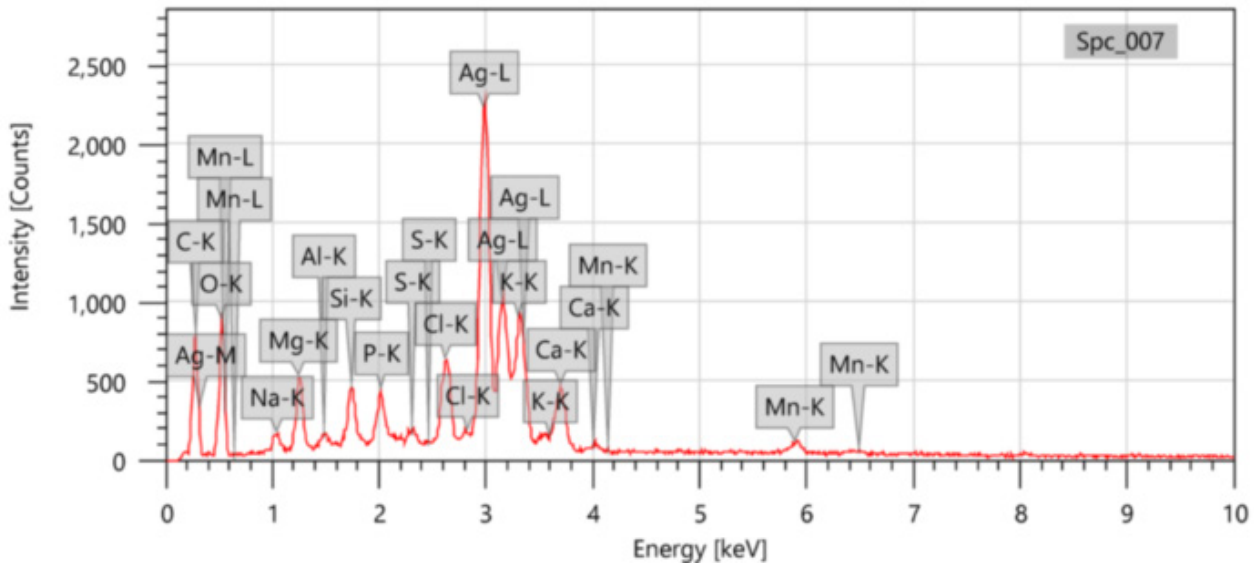

Figure 9: Energy Dispersive X-ray (EDX) image of *M. pauciflora* AgNPs.

features enhance their potential applicability in biomedical, environmental, and nanotechnological fields, where stability and monodispersity are crucial for predictable performance. DLS analysis further supported these observations. The measurement of hydrodynamic diameter and Polydispersity Index is widely recognized as a reliable method for characterizing plant-mediated silver nanoparticles.

TEM analysis

TEM was employed to examine the morphology, size, and dispersion of the synthesized Ag nanoparticles. TEM is widely regarded as a powerful tool for confirming nanoparticle dimensions and shapes with high accuracy (Dudkiewicz *et al*., 2011). In this study, TEM analysis showed that the *M. pauciflora* derived AgNPs were predominantly rectangular. Figures 11A-11C present both low- and high-magnification views of the nanoparticles. The high-magnification image clearly illustrates well-defined rectangular AgNPs with a uniform size distribution. As shown in Figure 11B, the particles measured approximately 12 nm, aligning closely with the size estimated from the XRD analysis. The consistency in particle size and shape is particularly important; as such, uniformity can significantly enhance the nanoparticles' electrical and optical characteristics. Similar findings are found in other studies. *Murdannia loriformis* synthesized AgNPs with a particle of size of 12.60±2.83 nm reported by Isa *et al*. (2023). This, in turn, makes them highly suitable for applications in biomedical, environmental, and nanotechnology fields.

Biological activities

Evaluation of cytotoxicity

The cytotoxic activity of *M. pauciflora*-derived AgNPs was evaluated against PANC-1 and HepG2 cancer cell lines at concentrations ranging from 100 to 500 µg/mL. The nanoparticles showed a mild, concentration-dependent inhibition toward the PANC-1 cell line, producing 20, 19, 17, 15, and 13% inhibition at the respective concentrations. From this trend, the IC_{50} value was calculated to be approximately 500 µg/mL, indicating relatively low cytotoxic potency. In contrast, no measurable cytotoxic effect was observed against the HepG2 liver cancer cell line at any of the tested concentrations, suggesting that the biosynthesized AgNPs from *M. pauciflora* may exhibit cell-line-specific activity, with a weak response limited to PANC-1 cells the cisplatin used as a standard drug. Previous studies reported that silver nanoparticles synthesized from *C. nudiflora* exhibited an IC_{50} value of 100 µg/mL against the HCT-116 colon cancer cell line (Kuppusamy *et al*., 2016). Additionally, various extracts of *C. benghalensis* including

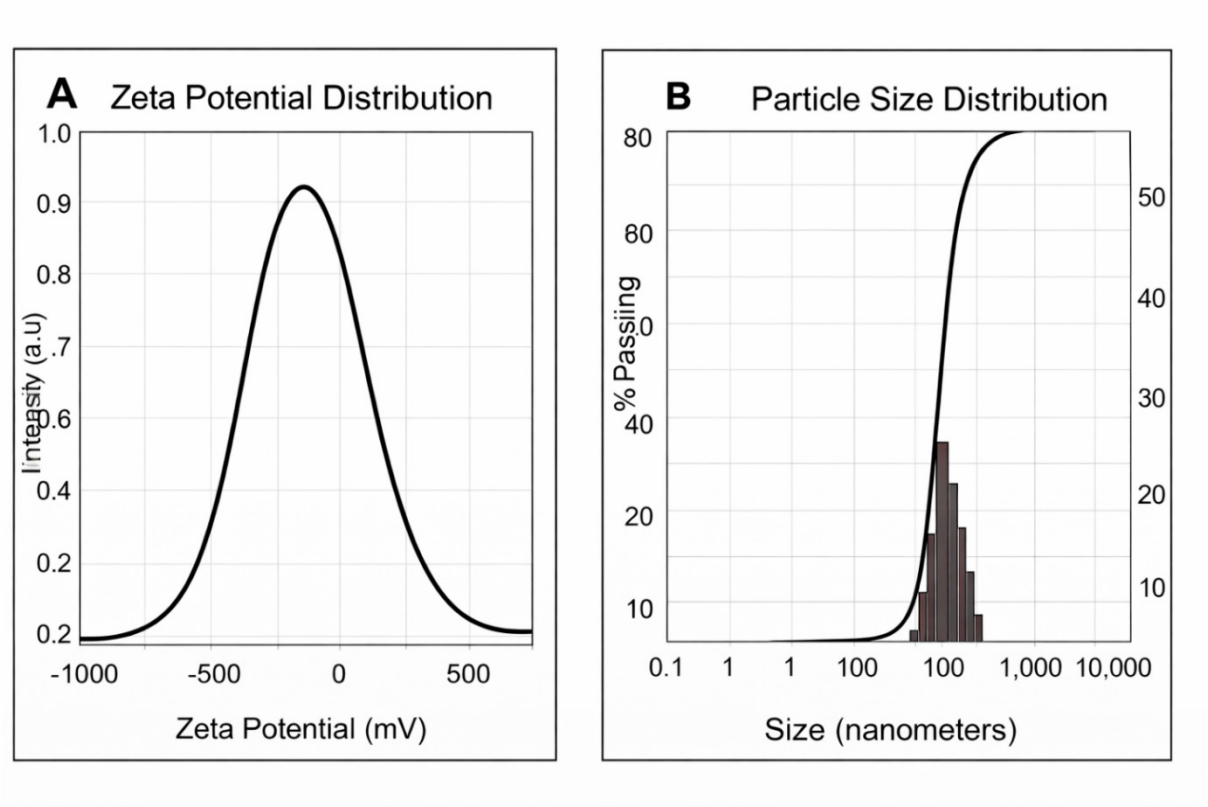

Figure 10: Dynamic Light Scattering (DLS) graph of *M. pauciflora* AgNPs.

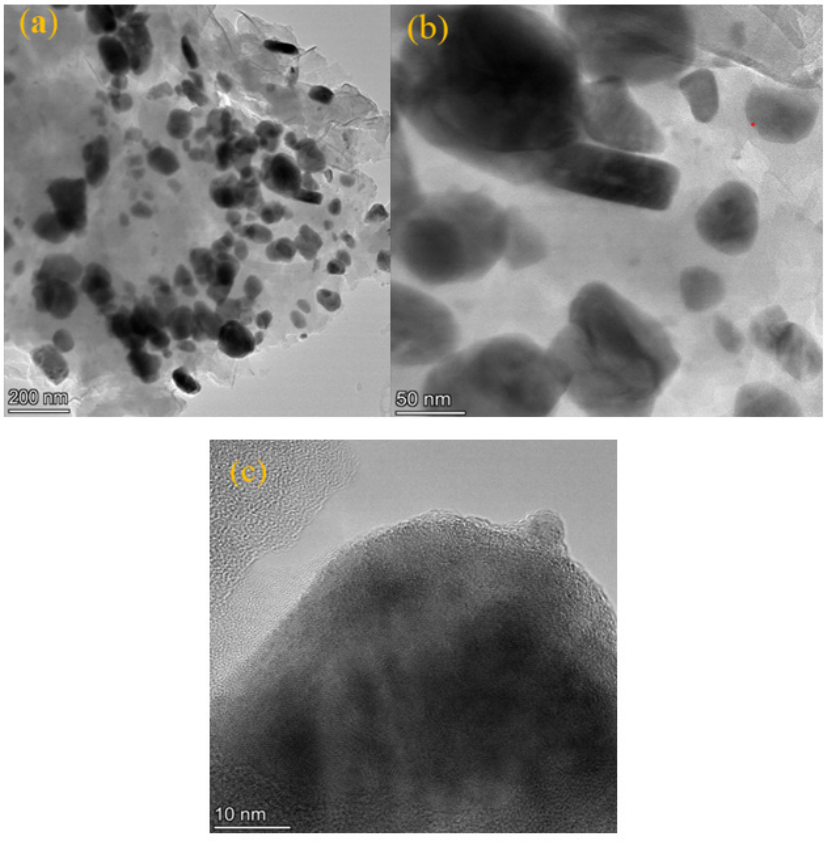

Figure 11: High Resolution Transmission Electron Microscopy (HR-TEM) of *M. pauciflora* AgNPs (A) Nanoparticles with a scale bar of 200 nm. (B) Close-up view of nanoparticles with a scale bar of 50 nm. (C) Detailed view showing a scale bar of 10 nm.

chloroform, methanol, n-hexane, benzene, and ethanol were tested against Hep-2 and MDA-MB-231 cancer cell lines. Among these, the chloroform extract showed the highest cytotoxicity against the breast cancer cell line MDA-MB-231 (Figures 12-18) (Batool *et al*., 2020).

Antidiabetic activity

α-glucosidase inhibition

The α-glucosidase assay showed that *M. pauciflora* AgNPs inhibit the enzyme in a clear concentration-dependent manner, with activity increasing from 8 to 66% between 20 and 100 µL. The IC_{50} value of 78.44 µg/mL indicates moderate inhibitory potential. In comparison, acarbose displayed stronger inhibition across all concentrations and with an IC_{50} of 30.57 µg/mL, confirming its higher potency. Despite this difference, the results suggest that biosynthesized AgNPs can interact with and suppress α-glucosidase activity, likely due to the combined effects of silver nanoparticles and the bioactive constituents of *M. pauciflora*. This indicates potential antidiabetic relevance. *Murdannia bracteata* showed a clear dose-dependent α-glucosidase inhibition, with an IC_{50} value of 117.04±2.34 µg/mL (Ooi *et al*., 2015). Similarly, the whole plant of *C. benghalensis* demonstrated notable antidiabetic effects in alloxan-induced diabetic rats (*"Antidiabetic activity and phytochemical investigation on the whole plant of Commelina benghalensis Linn. in male albino rat"*, 2016).

Antioxidant activity

DPPH assay

The free radical scavenging activity plays a vital role in protecting cells from oxidative damage. In this study, the antioxidant potential of biosynthesized *M. pauciflora* AgNPs was assessed using the DPPH assay. The nanoparticles showed a gradual, dose-dependent increase in scavenging activity, with inhibition values of 6, 20, 35, 47, and 61% at concentrations of 20, 40, 60, 80, 100, and IC_{50} value

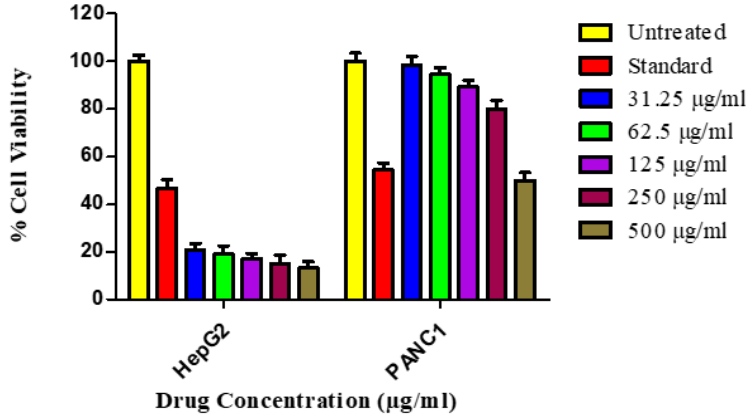

Figure 12: Cytotoxic assay showing different concentrations of *M. puaciflora* AgNPs against HepG2 and PANC1 cell line.

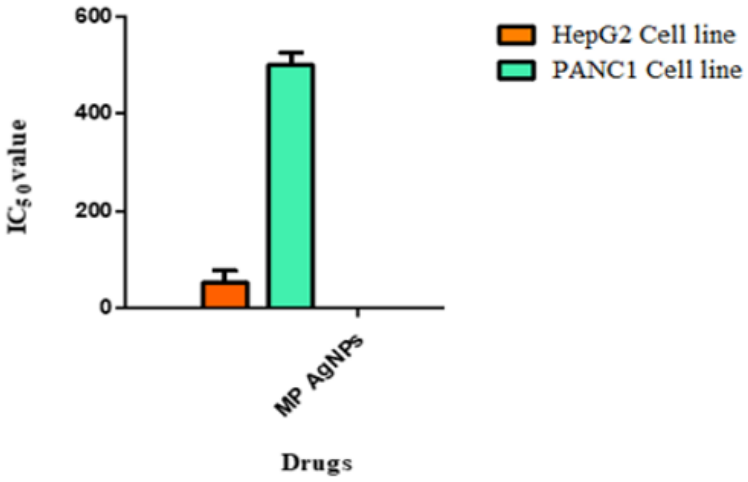

Figure 13: Showing cytotoxic assay of IC_{50} value of *M. pauciflora* against HepG2 and PANC1 cell line.

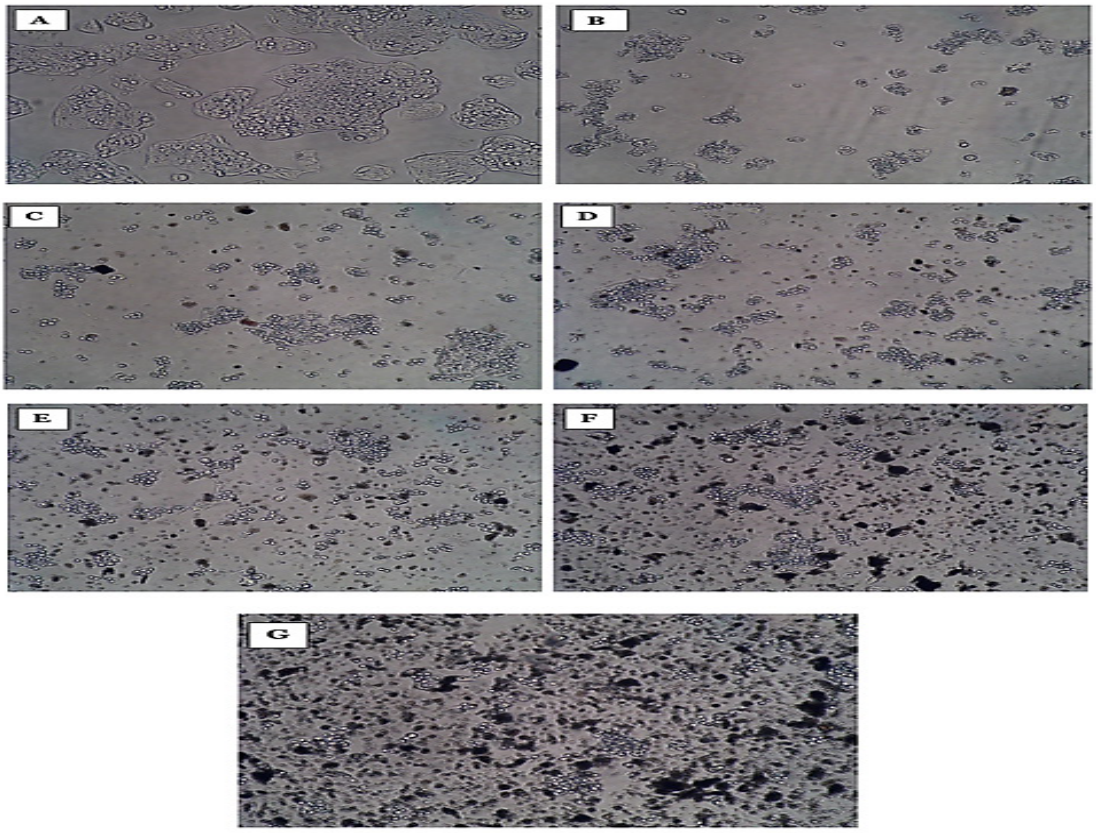

Figure 14: Microscopic images showing the cytotoxic effects (% cell viability) at different concentration of *M. pauciflora* AgNPs (A) Untreated (B) Standard (C) 31.25 µg/mL (D) 62.5 µg/mL (E) 125 µg/mL (F) 250 µg/mL (G) 500 µg/mL.

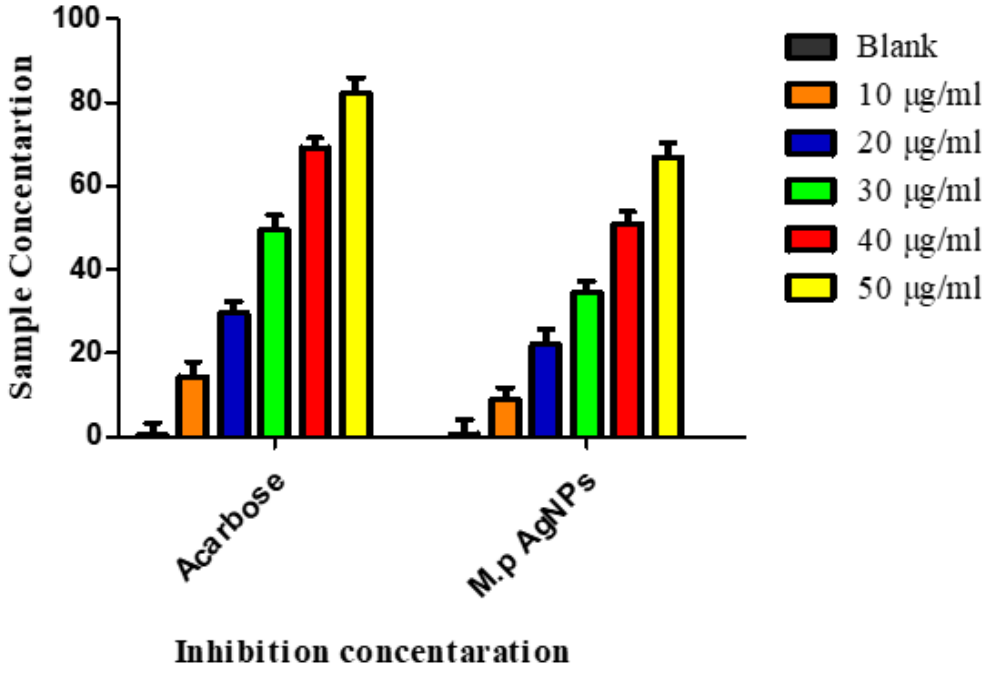

Figure 15: Antidiabetic activity showing different Concentrations of *M. pauciflora* AgNPs against SD Acarbose.

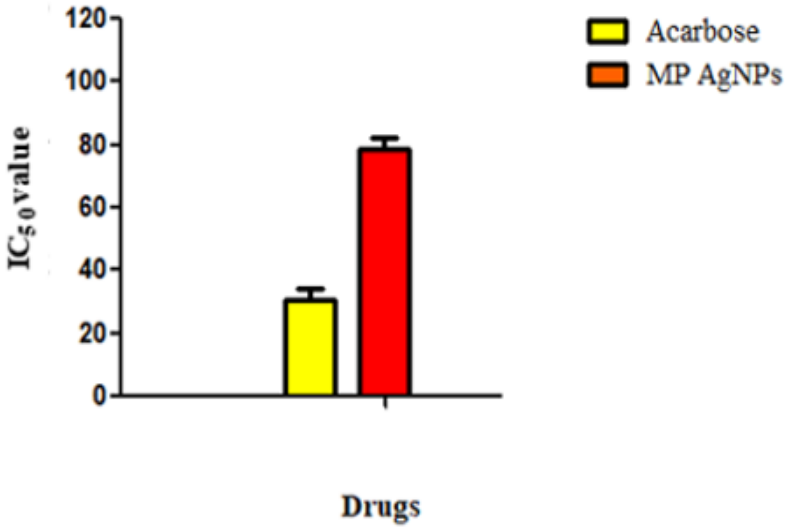

Figure 16: Showing α-glucosidase activity of IC_{50} value of *M. pauciflora* against SD. Acarbose.

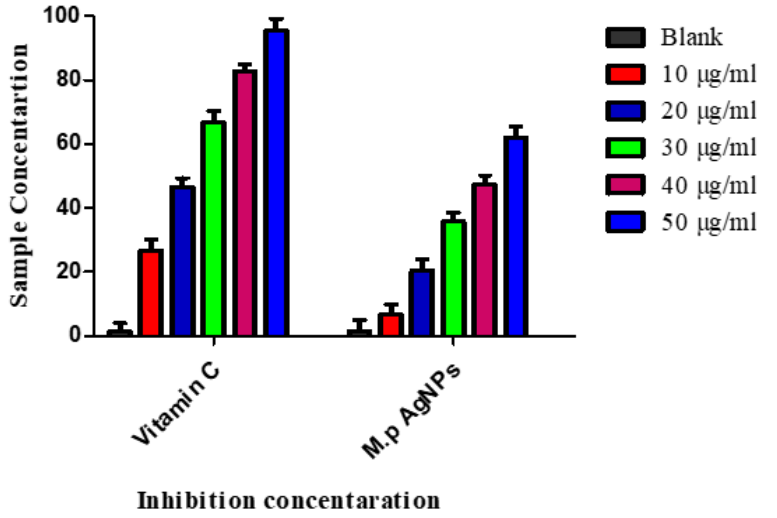

Figure 17: Antioxidant activity showing different Concentrations of *M. pauciflora* AgNPs against SD. Vitamin C.

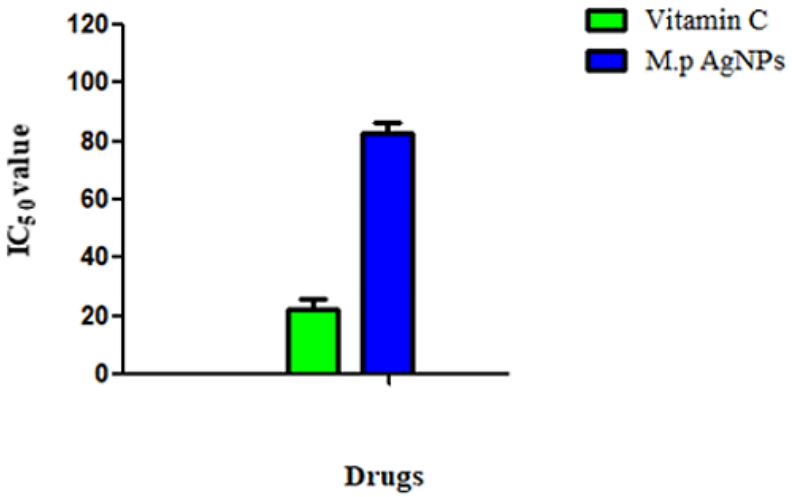

Figure 18: Antioxidant activity of IC_{50} value of *M. pauciflora* AgNPs against SD. Acarbose.

Table 3: Fourier-Transform Infrared (FTIR) Peak Values interpretation functional groups of *M. pauciflora* AgNPs.

Absorption (cm^{-1})	Intensities of functional group	Functional Group	Compound class
3,234.29	Strong, Sharp	O-H stretching	alcohol
3,138.63	Very Strong, Very Broad	O-H stretching	carboxylic acid
3,101.68	Medium to Weak	C-H stretching	aromatic hydrocarbon
3,005.20	Medium to weak	C-H stretching	aromatic hydrocarbon
2,957.99	Medium	C-H stretching	alkane
2,713.71	Medium	C-H stretching	aldehyde
2,251.84	Weak to Medium Sharp	N = C = O stretching	isocyanate
1,575.19	Medium	C = C stretching	cyclic alkane
1,393.37	Medium	O.-H. Bending	carboxylic acid
1,011.64	Strong, Sharp	S = O stretching	sulfoxide
780.18	Strong, Sharp	C-Cl stretching	alkyl halide
665.65	Strong	C = C. Bending	alkene

Abbreviations: C C. Bending.

of 82.65288 µg/mL, respectively. This increasing trend suggests that the AgNPs efficiently donate electrons to neutralize DPPH free radicals. Interestingly, their activity surpassed that of ascorbic acid, the positive control, recorded at IC_{50} value of 22.15 µg/mL (Graph 5). The strong antioxidant response may be attributed to phenolic and flavonoid compounds present in the plant extract, which likely act as capping agents on the nanoparticle surface. These phytochemicals facilitate the conversion of DPPH from purple to yellow, indicating effective radical quenching. Together, these findings highlight the potential of *M. pauciflora* AgNPs as promising natural antioxidants (Naaz *et al*., 2024). Reported that AgNPs synthesized from *Tradescantia pallida* showed a free radical scavenging activity with an IC_{50} value of 91.87 µg/mL. Similarly, AgNPs from *C. erecta* demonstrated strong antioxidant potential, with IC_{50} values of 69.92±1.01 µg/mL and 108.21 ±3.34 µg/mL (Mallick and Pradhan, 2024).

CONCLUSION

The present study successfully demonstrates, for the first time, the green synthesis of Silver Nanoparticles (AgNPs) using the aqueous extract of the ethnomedicinal plant *M. pauciflora*. The eco-friendly synthesis approach highlights the role of plant-derived phytochemicals as effective reducing and stabilizing agents, offering a sustainable alternative to conventional chemical methods. Phytochemical screening confirmed the presence of biologically active constituents such as phenols, flavonoids, alkaloids, tannins, glycosides, and saponins, while GC-MS analysis revealed a rich profile of 98 bioactive compounds that likely contributed to nanoparticle formation and biological activity. Comprehensive characterization using UV-visible spectroscopy, FTIR, XRD, SEM, EDX, DLS, zeta potential, and TEM confirmed the successful formation of stable and uniformly distributed AgNPs. The nanoparticles exhibited a face-centered cubic crystalline structure with a rectangular morphology, an average particle size of approximately 12 nm, and a surface charge of −30 mV, indicating good colloidal stability and reduced aggregation. These physicochemical properties are crucial for enhancing biological interactions and potential biomedical performance. Biological evaluations revealed that *M. pauciflora* AgNPs possess notable antioxidant and antidiabetic activities, as evidenced by their free radical scavenging and α-glucosidase inhibitory effects. The observed α-glucosidase inhibition, with a lower IC_{50} value compared to the standard, suggests their potential usefulness in managing postprandial hyperglycemia. Cytotoxicity studies against a pancreatic cancer cell line further demonstrated moderate anticancer potential, indicating that these nanoparticles may serve as promising candidates for future cancer-related applications. Overall, the findings of this study highlight the biomedical relevance of *M. pauciflora* mediated AgNPs and support their potential applications in antioxidant therapy, antidiabetic formulations, and targeted cancer treatment. Further *in vivo* studies and mechanistic investigations are warranted to validate their safety, efficacy, and clinical applicability.

ACKOWNLEDGEMENT

The authors sincerely thank the Chairman of the Department of Studies in Botany, Davangere University, Shivagangotri, Davangere, Karnataka, India, for sophisticated experimental and analytic facilities.

ABBREVIATIONS

AgNPs: Silver Nanoparticles; **BHT:** Butylated Hydroxytoluene; **BSS:** Balanced Salt Solution; **DLS:** Dynamic Light Scattering; **DMEM:** Dulbecco's Modified Eagle Medium; **DMSO:** Dimethyl Sulfoxide; **DPPH:** 2,2-diphenyl-1-picrylhydrazyl; **EDX:** Energy Dispersive X-ray; **FCC:** Face-Centered Cubic; **FTIR:** Fourier-Transform Infrared; **GC-MS:** Gas Chromatography-Mass Spectrometry; **HEPES:** 4-(2-hydroxyethyl)-1-p

iperazineethanesulfonic acid; **IC_{50}:** Half Maximal Inhibitory Concentration; **JCPDS:** Joint Committee on Powder Diffraction Standards; **MTT:** 3-(4,5-dimethylthiazol-2-yl)-2,5-diphenyltetrazolium bromide; **PDI:** Polydispersity Index; SEM: Scanning Electron Microscopy; SPR: Surface Plasmon Resonance; TEM: Transmission Electron Microscopy; **XRD:** X-ray Diffraction; **ZnO:** Zinc Oxide.

CONFLICT OF INTEREST

The authors declare that there is no conflict of interest.

REFERENCES

Abbigeri, M. B., Thokchom, B., Bhavi, S. M., Singh, S. R., Joshi, P., & Yarajarla, R. B. (2024). Potential *in vitro* antibacterial and anticancer properties of biosynthesized multifunctional silver nanoparticles using Martynia annua L. leaf extract. *Nano-Structures and Nano-Objects*, *39*, 101320. doi: 10.1016/j.nanoso.2024.101320.

Akintelu, S. A., Bo, Y., & Folorunso, A. S. (2020). A review on synthesis, optimization, mechanism, characterization, and antibacterial application of silver nanoparticles synthesized from plants. *Journal of Chemistry*, *2020*(1), 1-12. doi: 10.1155/2020/3189043.

Ali, S. G., Jalal, M., Ahmad, H., Sharma, D., Ahmad, A., Umar, K., & Khan, H. M. (2022). Green synthesis of silver nanoparticles from Camellia sinensis and its antimicrobial and antibiofilm effect against clinical isolates. *Materials*, *15*(19), 6978. doi: 10.3390/ma15196978.

Baliyan, S., Mukherjee, R., Priyadarshini, A., Vibhuti, A., Gupta, A., Pandey, R. P., & Chang, C. M. (2022). Determination of antioxidants by DPPH radical scavenging activity and quantitative phytochemical analysis of Ficus religiosa. *Molecules*, *27*(4), 1326. doi: 10.3390/molecules27041326.

Banu, K. S., & Cathrine, L. (2015). General techniques involved in phytochemical analysis. *International Journal of Advanced Research in Chemical Science*, *2*(4), 25-32.

Batool, R., Aziz, E., Iqbal, J., Salahuddin, H., Tan, B. H., Tabassum, S., & Mahmood, T. (2020). *In vitro* antioxidant and anti-cancer activities and phytochemical analysis of *Commelina benghalensis* L. root extracts. *Asian Pacific Journal of Tropical Biomedicine*, *10*(9), 417-425. doi: 10.4103/2221-1691.290133.

Bhav, S. M., Mirji, S. K., Thokchom, B., Singh, S. R., Maliger, R. B., Bhat, S. S., Jadidi, S. A. (2024). Potential antidiabetic properties of Syzygium Cumini (L.) Skeels leaf extract-mediated silver nanoparticles. *Austin Journal of Analytical and Pharmaceutical Chemistry*, *11*(1), 1168. doi: 10.26420/austinjanalpharmchem.2024.1168.

Bhavi, S. M., Padti, A. C., Thokchom, B., Singh, S. R., Bhat, S. S., Bajire, S. K., Yarajarla, R. B. (2024). Biogenic silver nanoparticles from Simarouba glauca DC leaf extract: Synthesis, characterization, and anticancer efficacy in lung cancer cells with protective effects in Caenorhabditis elegans. *Nano TransMed*, *3*, 100052. doi: 10.1016/j.ntm.2024.100052.

Bhavi, S. M., Thokchom, B., Abbigeri, M. B., Bhat, S. S., Singh, S. R., Joshi, P., & Yarajarla, R. B. (2024). Green synthesis, characterization, antidiabetic, antioxidant and antibacterial applications of silver nanoparticles from *Syzygium caryophyllatum* (L.) Alston leaves. *Process Biochemistry*, *145*, 89-103. doi: 10.1016/j.procbio.2024.06.017.

Bhavi, S. M., Thokchom, B., Singh, S. R., Bajire, S. K., Shastry, R. P., Srinath, B. S., Yarajarla, R. B. (2025). *Syzygium malaccense* leaf extract-mediated silver nanoparticles: Synthesis, characterization, and biomedical evaluation in Caenorhabditis elegans and lung cancer cell line. *Green Chemistry Letters and Reviews*, *18*(1), 2456624. doi: 10.1080/17518253.2025.2456624.

Chakraborty, B., Kumar, R. S., Almansour, A. I., Perumal, K., Nayaka, S., & Brindhadevi, K. (2022). *Streptomyces filamentosus* strain KS17 isolated from microbiologically unexplored marine ecosystems exhibited a broad spectrum of antimicrobial activity against human pathogens. *Process Biochemistry*, *117*, 42-52. doi: 10.1016/j.procbio.2022.03.010.

Dudkiewicz, A., Tiede, K., Loeschner, K., Jensen, L. H. S., Jensen, E., Wierzbicki, R., Molhave, K. (2011). Characterization of nanomaterials in food by electron microscopy. *TrAC Trends in Analytical Chemistry*, *30*(1), 28-43. doi: 10.1016/j.trac.2010.10.007.

Gudikandula, K., & Charya Maringanti, S. (2016). Synthesis of silver nanoparticles by chemical and biological methods and their antimicrobial properties. *Journal of Experimental Nanoscience*, *11*(9), 714-721. doi: 10.1080/17458080.2016.1139196.

Huq, S. (2015). *Comparative phytochemical evaluation and biological activity screening of Murdannia nudiflora and Tradescantia pallida*.

Isa, N., Mohamad, N. N., Mahmood, A., Bakhari, N. A., Mydin, M. M., & Arshad, N. M. (2023). *Formation and stability study of silver nanoparticles reduced by Murdania*

Jaast, S., & Grewal, A. (2021). Green synthesis of silver nanoparticles, characterization and evaluation of their photocatalytic dye degradation activity. *Current Research in Green and Sustainable Chemistry*, *4*, 100195. doi: 10.1016/j.crgsc.2021.100195.

Johnson, I., & Prabu, H. J. (2015). Green synthesis and characterization of silver nanoparticles by leaf extracts of Cycas circinalis, *Ficus amplissima*, *Commelina benghalensis* and *Lippia nodiflora*. *International Nano Letters*, *5*(1), 43-51. doi: 10.1007/s40089-014-0136-1.

RC, D., Karadakatti, P., Praveen, T., & Kakkalameli, S. B. (2024). *Biosynthesis of zinc oxide nanoparticles from Memecylon talbotianum D. Brandis leaf extract and its larvicidal activity*.

Khandel, P., Yadaw, R. K., Soni, D. K., Kanwar, L., & Shahi, S. K. (2018). Biogenesis of metal nanoparticles and their pharmacological applications: Present status and application prospects. *Journal of Nanostructure in Chemistry*, *8*(3), 217-254. doi: 10.1007/s40097-018-0267-4.

Kuppusamy, P., Ichwan, S. J. A., Al-Zikri, P. N. H., Suriyah, W. H., Soundharrajan, I., Govindan, N., Yusoff, M. M. (2016). *In vitro* anticancer activity of Au, Ag nanoparticles synthesized using *Commelina nudiflora* L. aqueous extract against HCT-116 colon cancer cells. *Biological Trace Element Research*, *173*(2), 297-305. doi: 10.1007/s12011-016-0666-7.

Kuppusamy, P., Yusoff, M. M., Ichwan, S. J. A., Parine, N. R., Maniam, G. P., & Govindan, N. (2015). *Commelina nudiflora* L. edible weed as a novel source for gold nanoparticles synthesis and studies on different physical-chemical and biological properties. *Journal of Industrial and Engineering Chemistry*, *27*, 59-67. doi: 10.1016/j.jiec.2014.11.045.

Lee, C. K., Fuse, S., Poopath, M., Pooma, R., & Tamura, M. N. (2022). Phylogenetics and infrafamilial classification of Commelinaceae (Commelinales). *Botanical Journal of the Linnean Society*, *198*(2), 117-130. doi: 10.1093/botlinnean/boab047.

Majeed, M., & Rather, M. A. (2024). Advancements in vitamin D encapsulation: Characterization, wall materials, and fortification applications. *Nutrire*, *49*(2), 48. doi: 10.1186/s41110-024-00292-5.

Malavika, J., & Thenmozhi, K. (2023). A comprehensive review on the ethnopharmacological and therapeutic perspectives of psychoactive plants. Kongunadu [Research journal], *10*(2), 48-52.

Mallick, S., Barik, D., & Pradhan, N. (2024a). *Commelina erecta*, L. biomass silver nanoparticle composite as a heterogeneous catalyst for methylene blue degradation. *Applied Catalysis O O*: *Open*, *192*, 206939. doi: 10.1016/j.apcato.2024.206939.

Mallick, S., Barik, D., & Pradhan, N. (2024b). *Commelina erecta*, L. biomass-silver nanoparticle composite as a heterogeneous catalyst for methylene blue degradation. *Applied Catalysis O: Open*, *192*, 206939.

Mallick, S., & Pradhan, N. (2024). Bio-fabrication of silver nanoparticles using *Commelina erecta*, L.: A mechanistic approach on synthesis, optimization, antibacterial, and antioxidant potential. *Bioprocess and Biosystems Engineering*, *47*(4), 495-507. doi: 10.1007/s00449-024-02980-y.

Mandour, Y. M., Refaat, E., & Hassanein, H. D. (2023). Anticancer activity, phytochemical investigation and molecular docking insights of *Citrullus colocynthis* (L.) fruits. *Scientific Reports*, *13*(1), 20038. doi: 10.1038/s41598-023-46867-6.

Mehta, B. K., Chhajlani, M., & Shrivastava, B. D. (2017, April). Green synthesis of silver nanoparticles and their characterization by XRD. In *Journal of Physics: Conference Series* (Vol. 836, No. 1, p. 012050). IOP Publishing, *836*, 012050. doi: 10.1088/1742-6596/836/1/012050.

Mohamad, N. N., Mahmood, A., Bakhari, N. A., Mydin, M. M., Arshad, N. M., & Isa, N. (2021, December). Studies on surface plasmon resonance of silver nanoparticles. In *Journal of Physics: Conference Series* (Vol. *2129*, No. 1, p. 012084). IOP Publishing, *2129*(1), 012084. doi: 10.1088/1742-6596/2129/1/012084.

Mukherji, S., & Mondal, D. (2017). Lab-on-chip (LOC) devices for point of care (POC) applications. In *Medical biosensors for point of care (POC) applications* (pp. 99-131). Woodhead Publishing. doi: 10.1016/B978-0-08-100072-4.00005-8.

Naaz, R., Siddiqui, V. U., Ahmad, A., Qadir, S. U., & Siddiqi, W. A. (2024). Study of antibacterial and antioxidant activities of silver nanoparticles synthesized from *Tradescantia pallida* (purpurea) leaves extract. *Journal of Dispersion Science and Technology*, *45*(5), 990-1000. doi: 10.1080/01932691.2023.2190394.

Nandikar, M. D., & Gurav, R. V. (2015). *Commelina badamica* (Commelinaceae), a new species from India. *Telopea*, *18*, 513-518. doi: 10.7751/telopea9256.

Nandikar, M. D., Kumbhalkar, B. B., & Gurav, R. V. (2018). GC-MS analysis of phytochemical compounds in the crude methanolic extract of roots of *Murdannia lanuginosa* and *M. simplex* (Commelinaceae). *Indian Journal of Natural Products and Resources (IJNPR) [Formerly Natural Product Radiance (NPR)]*, *9*(3), 229-234.

Nayaka, S., Chakraborty, B., Bhat, M. P., Nagaraja, S. K., Airodagi, D., Swamy, P. S., Kanakannanavar, B. (2020). Biosynthesis, characterization, and *in vitro* assessment on cytotoxicity of actinomycete-synthesized silver nanoparticles on Allium cepa root tip cells. *Beni-Suef University Journal of Basic and Applied Sciences*, *9*(1), 51. doi: 10.1186/s43088-020-00074-8.

Ooi, K. L., Loh, S. I., Tan, M. L., Muhammad, T. S. T., & Sulaiman, S. F. (2015). Growth inhibition of human liver carcinoma HepG2 cells and α-glucosidase inhibitory activity of *Murdannia bracteata* (CB Clarke) Kuntze ex JK Morton extracts. *Journal of Ethnopharmacology*, *162*, 55-60. doi: 10.1016/j.jep.2014.12.030.

Oseghale, C., Adedeji, K., Akoji, N., Abdullahi, K., Limangba, I. J., & Abimbola, O. F. (2025). *Green synthesis of Ag-Pt nanocatalysts from invasive Commelina diffusa for water purification: Toxicity and dual environmental benefits*. *Available at SSRN 5209185*.

P M, G., T R, V., L, V., Karadakatti, P., R C, D., & T, P. (2025). Studies on phytochemical screening and biological evaluation of Balanites Roxburghii planch: Cytotoxic and antibacterial activities. *Asian Journal of Research in Botany*, *8*(2), 643-651. doi: 10.9734/ajrib/2025/v8i2294.

Patrick, A. O., & Bakhari, N. A. (2020). A review of isolation and identification of bioactive components from Murdannia species. In 9th Virtual Science Invention Innovation Conference (SIIC) (pp. 170-172).

Praveen, T., & Kakkalameli, S. (2025a). Phytochemical profiling and biological activities of Strobilanthes urens (B. Heyne ex Roth) JRI wood. Leaf extract (Acanthaceae). *Sciences of Phytochemistry*, *4*(2), 107-115. doi: 10.58920/sciphy0402372.

Praveen, T., & Kakkalameli, S. B. (2025b). *Studies on phytochemical, GC-MS analysis in vitro cytotoxic assay and their biological Activities of Cynarospermum asperrimum (Nees) Vollesen*. (Acanthaceae).

PS, G. H., & Irchhaiya Raghuveer, D. V. A. (2016). Antidiabetic activity and phytochemical investigation on the whole plant of *Commelina benghalensis* Linn. in male albino rat. *Journal of Drug Delivery and Therapeutics*, *6*(2), 26-29.

RC, D., & Kakkalameli, S.B. (2025). *Phytochemical Screening, Proximate Analysis and Phyto-synthesis of zinc oxide Metallic Nanoparticles from the Leaf of Abutilon persicum* (Burm. F.) Merr. and their Biological Applications. *Authorea Preprints*.

Sheme, F. A., Aziz, M. A., Karim, M. R., Rahman, M. H., Rabbi, M. A., Nurujjaman, M., & Habib, M. R. (2023). Green preparation of silver nanoparticles using leaf extract of Amoora rohituka for antioxidant, antibacterial and anticancer applications. *Journal of Agriculture and Food Research*, *14*, 100889. doi: 10.1016/j.jafr.2023.100889.

Sukanya, D., Thanet, P., & Chatchai, W. (2017). Alpha-glucosidase inhibitory activity and phytochemical investigation of Borassus flabellifer Linn. *African Journal of Pharmacy and Pharmacology*, *11*(3), 45-52. doi: 10.5897/AJPP2016.4706.

Thokchom, B., Bhavi, S. M., Abbigeri, M. B., Shettar, A. K., & Yarajarla, R. B. (2023). Green synthesis, characterization and biomedical applications of Centella asiatica-derived carbon dots. *Carbon Letters*, *33*(4), 1057-1071. doi: 10.1007/s42823-023-00505-3.

Ujowundu, C. O., Igwe, C. U., Enemor, V. H. A., Nwaogu, L. A., & Okafor, O. E. (2007). Nutritive and anti-nutritive properties of Boerhavia diffusa and *Commelina nudiflora* leaves. *Pakistan Journal of Nutrition*, *7*(1), 90-92. doi: 10.3923/pjn.2008.90.92.

Vanajakshi, L., Arunakumara, V. P., Manjunath Gouda, P., Prashant Karadakatti, P. T., Darshan, R. C., Anju, S., Kotresha, D. (2025). Phytochemical Proiling and *in vitro* Evaluation of Biological Activities of Solanum diphyllum L. *Environmental reports; an international journal*.

Vanlalveni, C., Lallianrawna, S., Biswas, A., Selvaraj, M., Changmai, B., & Rokhum, S. L. (2021). Green synthesis of silver nanoparticles using plant extracts and their antimicrobial activities: A review of recent literature. *RSC Advances*, *11*(5), 2804-2837. doi: 10.1039/D0RA09941D.

Vijay, R., Drisya, V. M., Selta, D. R. F., Rathi, M. A., Gopalakrishnan, V. K., Alkhalifah, D. H. M., & Hozzein, W. N. (2023). Synthesis and characterization of silver nanomaterial from aqueous extract of *Commelina forskaolii* and its potential antimicrobial activity against Gram negative pathogens. *Journal of King Saud University - Science*, *35*(1), 102373. doi: 10.1016/j.jksus.2022.102373.

Xu, L., Wang, Y. Y., Huang, J., Chen, C. Y., Wang, Z. X., & Xie, H. (2020). Silver nanoparticles: Synthesis, medical applications and biosafety. *Theranostics*, *10*(20), 8996-9031. doi: 10.7150/thno.45413.

Cite this article: Vanajakshi L, Kotresha D. Bio-Fabrication of Silver Nanoparticles: *Murdannia pauciflora* (G. Brückn) Structural Analysis and Multifunctional Biological Properties. Asian J Biol Life Sci. 2026;15(2):530-48.